

Can WIMPs Survive a Magnetized Early Universe?

Malcolm Fairbairn,^{1,*} María Olalla Olea-Romacho,^{1,†} and Pranjal Ralegankar^{2,3,‡}

¹*Theoretical Particle Physics and Cosmology, King's College London, Strand, London WC2R 2LS, United Kingdom*

²*SISSA - International School for Advanced Studies, Via Bonomea 265, 34136 Trieste, Italy*

³*INFN - National Institute for Nuclear Physics, Via Valerio 2, I-34127 Trieste, Italy*

Primordial magnetic fields (PMFs) can seed additional small-scale matter fluctuations, leading to the formation of dense, early-collapsing dark matter structures known as minihalos. These minihalos may dramatically amplify the dark matter annihilation signal if dark matter is composed of self-annihilating thermal relic particles such as WIMPs. In this work, we explore the viability of this scenario by analysing the annihilation signal from minihalos with prompt central cusps, $\rho \propto r^{-3/2}$, formed due to the enhanced power spectrum induced by PMFs. Using observational constraints from the Virgo cluster and incorporating benchmark values for the magnetic field strength motivated by cosmological phase transitions such as the electroweak and QCD phase transitions, as well as the best-fit value from DESI and Planck data, we derive constraints on the dark matter annihilation cross section. We find that large portions of the WIMP parameter space are excluded, and magnetic fields produced during phase transitions with temperatures $T \lesssim 100$ GeV disfavour dark matter masses below 400 GeV. Notably, magnetic fields generated at or below the QCD phase transition scale, or with amplitudes favored by current cosmological data, are in strong tension with self-annihilating WIMPs across a wide mass range extending beyond the TeV scale. Our results establish indirect detection as a sensitive probe of the interplay between early-universe magnetogenesis and the microphysics of dark matter.

I. INTRODUCTION

Magnetic fields are observed on a wide range of astrophysical scales, from galaxies to galaxy clusters and the intergalactic medium [1–9]. Their origin, however, remains an open problem. One compelling possibility is that they were seeded by processes in the early universe, such as inflationary dynamics [10–15] or cosmological phase transitions [16–22]. If primordial magnetic fields (PMFs) exist, they may leave observable signatures on cosmological and astrophysical observables, including the cosmic microwave background [23–29], structure formation [30–52], and gravitational wave backgrounds [53–55]. Recently, PMFs have also been invoked to alleviate the Hubble tension between values of H_0 obtained through supernova observations and through observations of the CMB [56–59].

A consequence of PMFs is their ability to enhance the growth of small-scale matter perturbations [60]. Prior to recombination, the Lorentz force from a stochastic magnetic field induces compressible modes in the baryon fluid on scales smaller than the photon mean free path. While these baryonic perturbations can subsequently be erased by baryon thermal pressure, they leave a persistent gravitational imprint on the dark matter component. As a result, the dark matter power spectrum is amplified on small scales, potentially giving rise to a population of early-forming, compact minihalos [60].

In parallel, thermal relic dark matter candidates, such as weakly interacting massive particles (WIMPs), remain

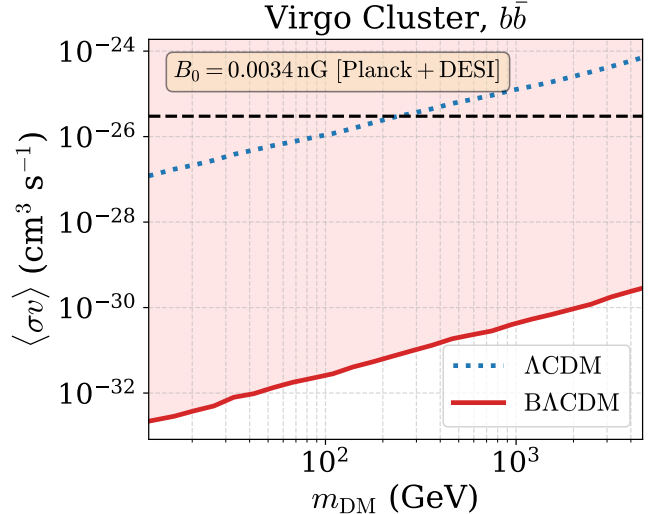


FIG. 1: Upper limits on the dark matter annihilation cross-section to $b\bar{b}$ final state in the Virgo cluster, considering a primordial magnetic field with present strength $B_0 = 3.4$ pG, corresponding to the best fit value from the combination of Planck CMB data and the baryon acoustic oscillation (BAO) measurements from the DESI Year 1 release [58]. Our limits rule out the thermal annihilation cross-section (black dashed) for dark matter masses extending beyond the TeV scale.

a key target of experimental efforts [61]. These particles are expected to self-annihilate, producing observable Standard Model final states, including gamma rays. However, in the standard cold dark matter (CDM) scenario, the annihilation signal from small-scale halos is typically suppressed by the late formation time and rel-

* malcolm.fairbairn@kcl.ac.uk

† maria.olalla.olea_romacho@kcl.ac.uk

‡ pralegan@sissa.it

actively shallow central profiles of low-mass halos.

This suppression can be overcome in scenarios with PMFs. The early formation of dark matter minihalos from sharp peaks in the enhanced power spectrum leads to the formation of *prompt cusps*: dense, centrally-concentrated structures with $\rho \propto r^{-3/2}$. These objects significantly enhance the annihilation rate and thus the expected gamma-ray signal, especially in environments such as galaxy clusters [62, 63].

In this work, we investigate the indirect detection prospects of self-annihilating dark matter in the presence of PMFs. Specifically, we analyze how PMF-induced prompt cusps modify the annihilation signal from the Virgo cluster, and use this to place constraints on the dark matter annihilation cross section. We consider three benchmark scenarios for the magnetic field strength: (i) a field generated at the QCD phase transition, (ii) a weaker field generated at the electroweak phase transition, and (iii) the best-fit field amplitude obtained from a joint analysis of Planck and DESI data [58] (see Fig. 1).

Generically, we find that the magnetic fields in the early universe places stringent constraints on the WIMP annihilation cross section. In particular, PMFs generated both around the QCD phase transition and also with cosmologically-motivated values exclude thermal WIMPs over a wide mass range extending beyond the TeV scale, potentially challenging their viability as dark matter candidates. For magnetic fields generated at the electroweak phase transition, we exclude thermal-relic WIMPs with masses $m_\chi \lesssim 300$ GeV, with constraints only marginally stronger than those obtained in standard Λ CDM without primordial magnetic fields [62]. More generally, magnetic fields produced at phase transition temperatures $T \lesssim 100$ GeV can exclude WIMPs with masses below 400 GeV, further tightening the bounds on the low-mass window. This work demonstrates that gamma-ray searches can be used to probe not only the properties of dark matter, but also the magnetic history of the early universe.

II. PRIMORDIAL MAGNETIC FIELDS AND MINIHALO FORMATION

Primordial magnetic fields can imprint significant features on the small-scale matter power spectrum [60]. A stochastic primordial magnetic field exerts a compressive Lorentz force on the baryon fluid. While baryons remain tightly coupled to the photon bath, relativistic photon pressure suppresses any growth on scales larger than the photon mean free path. However, below this scale, the coupling weakens, allowing the Lorentz force to drive baryonic inhomogeneities.

These baryonic overdensities may ultimately be erased by baryon thermal pressure. However, during the time in which the baryon fluctuations grow, they source gravitational potentials that also affect the dark matter component. Since dark matter is collisionless and does

not couple directly to photons or magnetic fields, it remains unaffected by baryon thermal pressure and retains the memory of these early gravitational perturbations.

As a result, the dark matter power spectrum is enhanced on small scales, even below the baryon Jeans length. The growth of the dark matter component continues uninterrupted after recombination, leading to the formation of compact, high-density dark matter structures at early times, commonly referred to as minihalos.

The abundance and internal structure of minihalos depend sensitively on the amplitude and shape of the enhanced power spectrum induced by the PMFs. In particular, PMFs with a Batchelor spectrum on large scales, $P_B(k) \propto k^2$, can lead to enhancements at sub-solar mass scales, potentially producing minihalos as light as $10^{-11} M_\odot$. The Batchelor spectrum is expected from PMFs generated in phase transition. Moreover, recent studies suggest that the subsequent turbulent evolution after phase transition enforces the Batchelor spectrum even if the initial field had a different spectrum [64].

This population of early-forming minihalos provides a novel probe of primordial magnetism, especially in scenarios where dark matter is self-annihilating, which is the subject of this paper. The initial collapse of these small-scale overdensities can lead to the formation of dense central regions known as prompt cusps, which play a key role in enhancing the indirect detection signal.

In this study, we connect the enhancement in the power spectrum to the initial PMF parameters using the analytical framework developed in Ref. [60]. A central assumption of this method is that the PMFs follow a Gaussian distribution. Given the possibility of non-Gaussianities in a realistic scenario, our findings should be regarded as order-of-magnitude estimates.

A key physical scale in this context is the free-streaming length of dark matter, which suppresses structure formation above a characteristic wavenumber k_{fs} . This suppression arises because dark matter particles decouple kinetically from the plasma at a finite temperature and retain residual velocities that erase small-scale perturbations through free-streaming. The free-streaming wavenumber k_{fs} depends on both the dark matter mass m_χ and the kinetic decoupling temperature T_{kd} [65]:

$$k_{\text{fs}} \approx 1.70 \times 10^6 \text{ Mpc}^{-1} \left(\frac{m_\chi}{100 \text{ GeV}} \right)^{1/2} \quad (1)$$

$$\times \left(\frac{T_{\text{kd}}}{30 \text{ MeV}} \right)^{1/2} \left[1 + \frac{\ln(T_{\text{kd}}/30 \text{ MeV})}{19.2} \right]^{-1}. \quad (2)$$

To account for this physical suppression in our calculation, we imposed a smooth cutoff on the matter power spectrum at k_{fs} , modeling it with the function

$$f(k) = \frac{1}{1 + \exp\left(\frac{k - k_{\text{fs}}}{\delta_k k_{\text{fs}}}\right)}, \quad (3)$$

where the parameter δ_k controls the smoothness of the cutoff.

In all our results, we fixed the kinetic decoupling temperature at $T_{\text{kd}} = 30 \text{ GeV}$. Realistic dark matter models that evade current direct detection constraints often feature early kinetic decoupling. For instance, pseudo Nambu–Goldstone boson dark matter models [66, 67], which naturally suppress tree-level scattering with nuclei, can exhibit kinetic decoupling temperatures comparable to or even exceeding the freeze-out temperature [68]. Moreover, since the annihilation signal depends only logarithmically on T_{kd} , our results are only mildly sensitive to this parameter: for benchmark magnetic field strengths of order pG, varying T_{kd} from 30 MeV to 30 GeV changes the cross-section constraints by at most $\sim 160\%$ and by as little as $\sim 12\%$ across the full dark matter mass range. This mild dependence reflects the fact that the properties of prompt cusps are mainly dictated by the scale of the power spectrum enhancement, rather than by the free-streaming cutoff.

III. PROMPT CUSPS PROPERTIES

Prompt cusps are dense, power-law central structures that form during the monolithic (i.e. not hierarchical) collapse of isolated peaks in the early dark matter density field. Unlike the more familiar Navarro-Frenk-White (NFW) halos, which arise from hierarchical structure formation and exhibit a characteristic core-like inner slope ($\rho \propto r^{-1}$), prompt cusps develop an inner density profile of $\rho \propto r^{-3/2}$ [63, 69]. This profile forms quasi-instantaneously at the moment of collapse and is tightly determined by the local properties of the linear density peak, particularly its amplitude and curvature. The prompt cusp persists at the center of the resulting halo even as it later accretes additional material and grows an NFW-like outer envelope [63].

Importantly, while in ΛCDM cosmologies the smallest halos form at the free-streaming scale k_{fs} , in PMF cosmologies it is the scale of the spectral bump that determines the first structures to collapse, as it is the first to become non-linear. This is because the bump injects a localized excess of power at scales larger than the free-streaming length, boosting the density contrast sufficiently for those perturbations to reach the collapse threshold earlier than any others. As a result, the earliest minihalos form around the bump scale rather than the free-streaming cutoff. In particular, the gravitational influence of magnetically induced baryon inhomogeneities seeds dark matter perturbations on these intermediate scales, enhancing the abundance of low-mass minihalos, and increasing the likelihood that they form prompt cusps: dense, centrally concentrated structures with $\rho \propto r^{-3/2}$ [60].

Each prompt cusp forms with a density profile $\rho = Ar^{-3/2}$ extending between an inner core radius r_{core} , imposed by phase-space constraints, and an outer cusp radius r_{cusp} , determined by the peak size. Since the annihilation rate formally diverges at small radii in a density

profile that scales as $\rho \propto r^{-3/2}$, understanding the inner structure of prompt cusps is essential. Analytical arguments [70], supported approximately by numerical simulations [71], indicate that the initial thermal motion of dark matter particles imposes a finite-density core at the center of the cusp. The radius of this core, r_{core} , is given by

$$r_{\text{core}} \simeq 0.34 G^{-2/3} \left(\frac{m_\chi}{T_{\text{kd}}} \right)^{-2/3} \bar{\rho}(a_{\text{kd}})^{-4/9} A^{-2/9}, \quad (4)$$

where $\bar{\rho}(a_{\text{kd}})$ is the mean dark matter density at the time of kinetic decoupling, and A is the normalization of the cusp density profile

$$\rho = Ar^{-3/2}. \quad (5)$$

The coefficient A can be statistically predicted from the linear power spectrum [69]:

$$A \simeq 24 \bar{\rho}(a_{\text{coll}}) (a_{\text{coll}} R)^{3/2}. \quad (6)$$

and is set by the collapse time a_{coll} and characteristic comoving size R . The scale factor at collapse a_{coll} is estimated using the ellipsoidal collapse approximation in Ref. [72], and the characteristic comoving size is given by $R \equiv |\delta/\nabla^2\delta|^{1/2}$, where δ is the height of the peak in the density contrast and $\nabla^2\delta$ is the Laplacian of the density contrast with respect to the comoving position. This cusp profile extends out to a radius set by the comoving size of the collapsing density peak and its collapse time, and is given by [69]

$$r_{\text{cusp}} \simeq 0.11 a_{\text{coll}} R. \quad (7)$$

These structures are the densest dark matter configurations expected in a CDM universe and are predicted to survive hierarchical merging and tidal stripping with their inner structure largely intact [63]. Since we will be studying the signal from the halos of clusters of galaxies, rather than within galactic halos themselves, we do not expect significant tidal disruption.

To model the properties of prompt cusps seeded by enhanced small-scale fluctuations, we make use of the publicly available code developed in [69, 70], which samples halo populations from a given matter power spectrum. The code implements the BBKS peak statistics formalism [73] and uses the ellipsoidal collapse criterion to determine whether a peak collapses to form a prompt cusp. For each collapsing peak, it predicts the asymptotic density profile.

IV. ANNIHILATION SIGNAL

The steep inner density profiles of prompt cusps significantly enhance the dark matter annihilation rate relative to standard halo models. The high central densities of these structures result in substantial contributions to

the annihilation signal, even though the cusps themselves comprise only a small fraction of the total dark matter mass (around the 5%).

To quantify the contribution of prompt cusps to the annihilation signal, we follow the formalism introduced in [63] and developed in [62]. The gamma-ray flux from dark matter annihilation reads

$$\frac{d^2\Phi}{d\Omega dE} = \frac{\langle\sigma v\rangle}{8\pi m_\chi^2} \frac{dN_\gamma}{dE} \frac{dJ}{d\Omega}. \quad (8)$$

Here $\langle\sigma v\rangle$ is the thermally averaged annihilation cross section, and dN_γ/dE is the gamma-ray spectrum per annihilation. The astrophysical contribution is encoded in the J-factor, which in our case includes both the smooth halo and the contribution from surviving prompt cusps

$$\frac{dJ}{d\Omega} = \int dl \rho(r) [\rho(r) + f_{\text{surv}} f_{\text{tidal}}(r) \rho_{\text{eff},0}], \quad (9)$$

integrated over the line-of-sight l . Here, $\rho(r)$ is the smooth density profile of the host halo (for which we adopt an NFW profile), and the second term captures the contribution from embedded prompt cusps. The parameter $f_{\text{surv}} \sim 0.5$ accounts for the fraction of cusps that survive tidal disruption after accretion into larger structures [63], and $\rho_{\text{eff},0}$ is the effective annihilation density of the initial population of cusps. The quantity $\rho_{\text{eff},0}$ is computed by statistically sampling the cusp population from the enhanced matter power spectrum, following the procedure outlined in the previous section.

The average contribution of the prompt cusps per mass of dark matter is:

$$\rho_{\text{eff},0} \equiv \frac{\int_{\text{cusps}} \rho^2 dV}{M} = n_{\text{peaks}} \langle j \rangle / \bar{\rho}_0, \quad (10)$$

where n_{peaks} is the comoving number density of collapsed dark matter structures that form from individual peaks in the linear density field [69], and $\rho_0 \simeq 33 M_\odot \text{kpc}^{-3}$. We sampled $N = 10^4$ density peaks, and averaged over the population to obtain $\langle j \rangle$ defined through

$$j \equiv \int_{\text{cusp}} \rho^2 dV = 4\pi A^2 [1/3 + \ln(r_{\text{cusp}}/r_{\text{core}})]. \quad (11)$$

In our analysis, we focus on the Virgo cluster as the observational target. This choice is motivated by the results in [62], which show that Virgo provides the most stringent constraints among the galaxy clusters analysed. For Virgo, we adopt a NFW profile with scale radius $r_s = 335.10 \text{kpc}$, scale density $\rho_s = 305646 M_\odot \text{kpc}^{-3}$ [74]. The cluster is located at a distance $d_L = 15.46 \text{Mpc}$ and subtends an angle by the virial radius $\theta_{200} = 6.32 \text{deg}$ [74].

We neglected the radial suppression factor $f_{\text{tidal}}(r)$ that accounts for tidal stripping of cusps in the inner regions of the host halo, given that its total annihilation signal is relatively modest, of order 5%, and does not significantly affect the derived constraints [62].

By combining our estimate of $\rho_{\text{eff},0}$ from the enhanced power spectrum with the Virgo cluster profile, we compute the integrated J factors and derive constraints on the annihilation cross section as a function of the dark matter mass, by rescaling the results in Ref. [62].

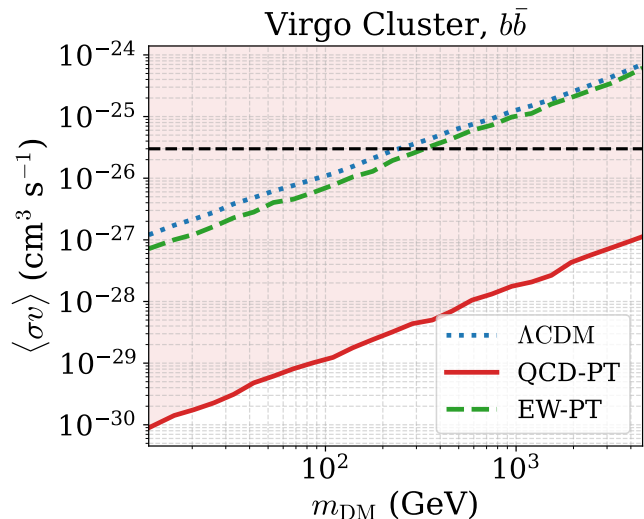


FIG. 2: Upper limits on the dark matter annihilation cross-section to a $b\bar{b}$ final state in the Virgo cluster, assuming a primordial magnetic field generated at the QCD phase transition (QCD-PT, red) or at the electroweak phase transition (EW-PT, green dashed). The ΛCDM baseline (blue dotted) and the canonical thermal cross-section (black dashed) are shown for comparison. The QCD-PT scenario yields the strongest bounds, ruling out thermal WIMPs up to multi-TeV masses.

V. RESULTS

Here we discuss our results for the annihilation cross section constraints derived from the enhanced small-scale matter power spectrum induced by PMFs, as traced by the dark matter annihilation signal from the Virgo cluster. We focus on annihilation into the $b\bar{b}$ channel, since it yields the strongest constraints [62]. Furthermore, we assume the non-helical magnetic fields evolve via reconnection dynamics for plasma kinetic Reynolds numbers greater than unity ($Re > 1$) and under viscous damping for smaller Reynolds numbers ($Re < 1$). Note that helical fields could lead to larger magnetic field strengths at the time of minihalo formation, potentially resulting in stronger constraints on dark matter annihilation.

Fig. 1 shows the upper limits on the dark matter annihilation cross-section into $b\bar{b}$ final states in the Virgo cluster, assuming a primordial magnetic field with present-day strength $B_0 = 0.0034 \text{nG}$, corresponding to the best-fit value from the combination of Planck CMB data and DESI Year 1 BAO measurements [58]. The red curve

shows the results in the $b\Lambda$ CDM model, defined as a minimal extension of Λ CDM by a single additional parameter: the comoving magnetic field strength at the onset of structure formation. The magnetic field coherence length is set by MHD turbulence, as mentioned above.

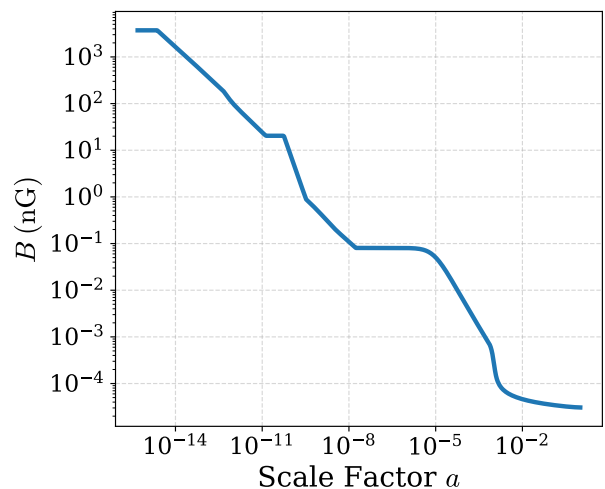
Compared to the standard Λ CDM scenario (blue dashed line) [62], adding a primordial magnetic field enhances the small-scale structure and leads to significantly stronger gamma-ray constraints. In this scenario, annihilation cross-sections are excluded up to six orders of magnitude below the thermal relic cross section (black dashed line), across the full dark matter mass range from below 10 GeV to above 4 TeV. The improvement in the fit to Planck and DESI data between $b\Lambda$ CDM and Λ CDM corresponds to $\Delta\chi^2 = -4.7$ (approximately a 2σ preference), and the resulting impact on indirect detection constraints is significant.

Fig. 2 illustrates two benchmark scenarios for primordial magnetic fields generated at the QCD and electroweak phase transitions. For the electroweak-scale magnetogenesis case, we assume magnetic fields are produced at $T_{\text{PT}} = 160$ GeV with maximal energy density, i.e., $\rho_B = \rho_{\text{SM}}$, and coherence length ξ equal to the horizon size at that time, $\xi = (aH)^{-1}$. This choice represents an optimistic upper bound, as more realistic magnetogenesis scenarios are expected to yield smaller field strengths.

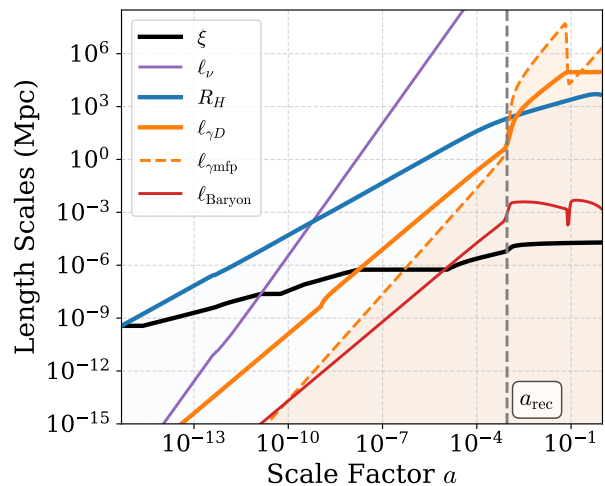
Figure 3 shows the evolution of the magnetic field strength and coherence length after electroweak magnetogenesis. The evolution has two distinct regimes. The first regime corresponds to when the plasma kinetic Reynolds number (Re) is above unity. During this time, the field undergoes a turbulent inverse cascade that conserves the Hosking integral ($B^4\xi^5 = \text{const}$ [75]), with a coherence scale of $\xi \sim \frac{0.1V_A}{aH}$, where V_A is the Alfvén speed (see Ref. [76] for details about V_A).

The second stage, a viscous damping regime, begins when Re falls below unity, i.e. when the coherence scale is surpassed by the photon or neutrino free-streaming scales. This transition leads to a temporary pause in the evolution, visible in Fig. 3, caused by the suppression of turbulence from the viscous drag of photons/neutrinos. The evolution restarts once the viscous damping scale, $\xi_D \sim \frac{V_A}{a\sqrt{(l_{\text{mfp}}^{-1}+H)H}}$, grows larger than the initial coherence scale [76]. Here l_{mfp} is the photon/neutrino mean free path. Note that we assume the Hosking integral is not conserved in the viscous regime, and instead assume $B^2\xi^5 = \text{const}$.¹ This viscous period ends when the photon/neutrino diffusion scale exceeds the horizon size and the plasma’s turbulence is restored.

Under these assumptions, magnetic field generation at the electroweak phase transition leads to a present-day



(a) Evolution of the comoving magnetic field strength B as a function of the scale factor a .



(b) Evolution of the magnetic coherence length scale ξ (black) alongside other characteristic length scales: neutrino diffusion $l_{\nu D}$, horizon $R_H \equiv (aH)^{-1}$, photon diffusion $l_{\gamma D}$, photon mean free path $l_{\gamma \text{mfp}}$, and baryon thermal pressure scale l_{Baryon} . PMFs evolve under viscous damping when $R_H > l_{\nu D} > \xi$ or $R_H > l_{\gamma D} > \xi$. PMFs can enhance the baryon and dark matter density perturbations when ξ is inside the orange shaded region.

FIG. 3: Cosmological evolution of the magnetic field and relevant length scales for a field generated at a benchmark electroweak phase transition occurring at $T_{\text{PT}} = 160$ GeV.

comoving magnetic field strength of $B_0 \approx 3.06 \times 10^{-5}$ nG. As seen in Fig. 2, this field induces a modest enhancement of the J -factor. Consequently, the electroweak magnetogenesis scenario (green curve) excludes the canonical thermal relic cross section only for dark matter masses up to $m_\chi \lesssim 300$ GeV, resulting in constraints that are only marginally stronger than those of standard Λ CDM without primordial magnetic fields (blue dashed). Fu-

¹While the conservation of the Hosking integral in the viscous regime remains an open theoretical question, we adopt $B^2\xi^5 = \text{const}$ in line with the treatment of Ref. [60], where this assumption was used to estimate enhancements to the dark matter power spectrum.

ture indirect detection constraints on the WIMP annihilation signal for higher mass WIMPs are expected from the Cerenkov Telescope Array [77].

For the QCD-scale magnetogenesis scenario, we assume that magnetic fields are generated at $T_{\text{PT}} = 150 \text{ MeV}$ with maximal energy density, $\rho_B = \rho_{\text{SM}}$, and a coherence length equal to the horizon size at that time, $\xi = (aH)^{-1}$. Under the ΛCDM hypothesis (red curve), this enhancement of small-scale power increases the J-factor by roughly five orders of magnitude relative to standard ΛCDM , thereby excluding the canonical thermal-relic cross section for dark matter masses from below 10 GeV up to beyond 4 TeV.

These two benchmark scenarios demonstrate that even sub-nanogauss magnetic fields, naturally arising from cosmological phase transitions, can significantly enhance the small-scale matter power spectrum. This enhancement, in turn, leads to the early formation of dense minihalos with prompt cusps, and can result in a substantial boost to the dark matter annihilation rate.

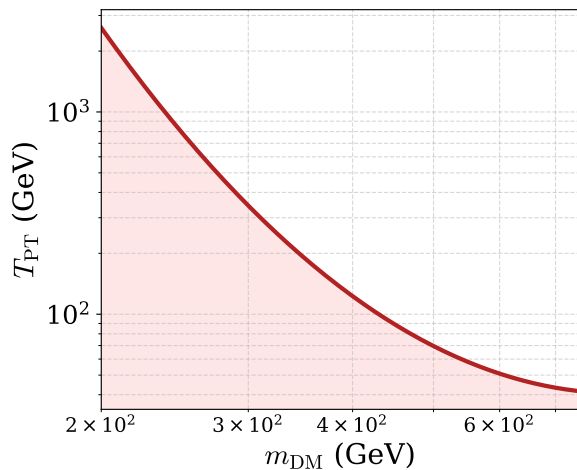


FIG. 4: Lower bound on the temperature of the phase transition T_{PT} as a function of the dark matter mass m_{DM} , assuming that the magnetic energy density at generation equals that of the Standard Model plasma. For a given dark matter mass, values of T_{PT} below the curve are excluded under the assumption of thermal-relic annihilation.

To generalise beyond these benchmarks, Fig. 4 shows the lower bound on the temperature of the phase transition, T_{PT} , as a function of the dark matter mass, m_{DM} . As in the benchmark scenarios discussed above, this analysis assumes that the primordial magnetic field is generated at a phase transition with energy density equal to that of the Standard Model plasma and a coherence length of the order of the horizon size. The resulting magnetic field strength is constrained by indirect detection limits, under the assumption of a thermal-relic annihilation cross section. For phase transitions occurring at $T_{\text{PT}} \lesssim 100 \text{ GeV}$, dark matter masses below 400 GeV

are excluded in this setup. This bound delineates the viable region for magnetogenesis from phase transitions in scenarios where dark matter is a thermal WIMP.

VI. CONCLUSIONS

In this study, we have investigated how primordial magnetic fields (PMFs) enhance the small-scale matter power spectrum, leading to the early formation of dense dark matter minihalos with prompt central cusps. These cusps, characterized by steep inner density profiles scaling as $\rho \propto r^{-3/2}$, result in a significant enhancement of the dark matter annihilation rate due to their extreme central densities.

By modeling the abundance and structure of the prompt cusps using peak statistics and ellipsoidal collapse, and comparing the predicted annihilation signal to gamma-ray observations from the Virgo cluster, we have derived constraints on the annihilation cross section of self-annihilating dark matter. Our analysis spans three benchmark cases for the comoving magnetic field strength: those associated with magnetogenesis during the QCD and electroweak phase transitions, and the best-fit value inferred from DESI and Planck data.

We find that the presence of primordial magnetic fields is in strong tension with the thermal WIMP hypothesis. In particular, magnetic fields generated at the QCD phase transition induce such an efficient production of prompt cusps that the resulting annihilation signal exceeds current observational limits over a broad mass range, from below 10 GeV to above 4 TeV. Similarly, magnetic fields with amplitudes matching the best-fit values from DESI and Planck are sufficient to exclude thermal WIMPs across the entire mass range considered. This suggests that the magnetic fields favored by current CMB observations are incompatible with scenarios in which dark matter is a self-annihilating thermal relic. Even in the more conservative case of PMFs generated during the electroweak phase transition, thermal WIMPs with masses below approximately 300 GeV are ruled out leaving only the high-mass regime within reach of future indirect detection experiments such as Cerenkov Telescope Array [77].

In addition, we have presented a complementary constraint based on the energy scale of the phase transition responsible for PMF generation. Assuming that the magnetic field is produced at a transition with an energy density equal to that of the Standard Model plasma and the coherence length at production is of the order of the horizon size, we compute the resulting magnetic field strength and determine the corresponding gamma-ray signal under the assumption of a thermal annihilation cross section. As shown in Fig. 4, for each value of the dark matter mass, temperatures below the exclusion curve are ruled out, since they would produce fields strong enough to generate prompt cusps that overproduce the annihilation signal. This result outlines the

viable parameter space for phase transitions that could be responsible for primordial magnetogenesis in scenarios involving thermally produced dark matter.

Our findings highlight the power of indirect detection not only to constrain the microscopic properties of dark matter but also to probe the early-universe processes that could have seeded cosmic magnetic fields. If intergalactic magnetic fields are indeed primordial in origin, they offer a natural amplification mechanism for dark matter annihilation signatures, thereby leading to a new obser-

vational link between particle physics and cosmological magnetogenesis.

ACKNOWLEDGMENTS

MF and MOOR are supported by the STFC under UKRI grant ST/X000753/1.

-
- [1] A. Neronov and I. Vovk, *Science* **328**, 73 (2010), <https://www.science.org/doi/pdf/10.1126/science.1184192>.
- [2] A. Abramowski *et al.* (H.E.S.S.), *Astron. Astrophys.* **562**, A145 (2014), arXiv:1401.2915 [astro-ph.HE].
- [3] J. D. Finke, L. C. Reyes, M. Georganopoulos, K. Reynolds, M. Ajello, S. J. Fegan, and K. McCann, *Astrophys. J.* **814**, 20 (2015), arXiv:1510.02485 [astro-ph.HE].
- [4] S. Archambault *et al.* (VERITAS), *Astrophys. J.* **835**, 288 (2017), arXiv:1701.00372 [astro-ph.HE].
- [5] R. Alves Batista and A. Saveliev, *Universe* **7**, 223 (2021), arXiv:2105.12020 [astro-ph.HE].
- [6] V. A. Acciari *et al.* (MAGIC), *Astron. Astrophys.* **670**, A145 (2023), arXiv:2210.03321 [astro-ph.HE].
- [7] I. Vovk, A. Korochkin, A. Neronov, and D. Semikoz, *Astron. Astrophys.* **683**, A25 (2024), arXiv:2306.07672 [astro-ph.HE].
- [8] J. Tjemsland, M. Meyer, and F. Vazza, *Astrophys. J.* **963**, 135 (2024), arXiv:2311.04273 [astro-ph.HE].
- [9] A. E. Broderick, P. Chang, and C. Pfrommer, *Astrophys. J.* **752**, 22 (2012), arXiv:1106.5494 [astro-ph.CO].
- [10] B. Ratra, *Astrophys. J. Lett.* **391**, L1 (1992).
- [11] M. S. Turner and L. M. Widrow, *Phys. Rev. D* **37**, 2743 (1988).
- [12] T. Kobayashi, *JCAP* **05**, 040 (2014), arXiv:1403.5168 [astro-ph.CO].
- [13] R. Durrer, L. Hollenstein, and R. K. Jain, *JCAP* **03**, 037 (2011), arXiv:1005.5322 [astro-ph.CO].
- [14] R. Sharma, K. Subramanian, and T. R. Seshadri, *Phys. Rev. D* **97**, 083503 (2018), arXiv:1802.04847 [astro-ph.CO].
- [15] K. Yanagihara, F. Uchida, T. Fujita, and S. Tsujikawa, *Phys. Rev. D* **110**, 083506 (2024), arXiv:2312.07938 [astro-ph.CO].
- [16] T. Vachaspati, *Phys. Lett. B* **265**, 258 (1991).
- [17] J. Ellis, M. Fairbairn, M. Lewicki, V. Vaskonen, and A. Wickens, *JCAP* **09**, 019 (2019), arXiv:1907.04315 [astro-ph.CO].
- [18] M. O. Olea-Romacho, *Phys. Rev. D* **109**, 015023 (2024), arXiv:2310.19948 [hep-ph].
- [19] J. M. Quashnock, A. Loeb, and D. N. Spergel, *Astrophys. J. Lett.* **344**, L49 (1989).
- [20] G. Sigl, A. V. Olinto, and K. Jedamzik, *Phys. Rev. D* **55**, 4582 (1997), arXiv:astro-ph/9610201.
- [21] J. Yang and L. Bian, *Phys. Rev. D* **106**, 023510 (2022), arXiv:2102.01398 [astro-ph.CO].
- [22] Y. Di, J. Wang, R. Zhou, L. Bian, R.-G. Cai, and J. Liu, *Phys. Rev. Lett.* **126**, 251102 (2021), arXiv:2012.15625 [astro-ph.CO].
- [23] P. Trivedi, J. Reppin, J. Chluba, and R. Banerjee, *Mon. Not. Roy. Astron. Soc.* **481**, 3401 (2018), arXiv:1805.05315 [astro-ph.CO].
- [24] D. Paoletti, J. Chluba, F. Finelli, and J. A. Rubiño Martín, (2022), 10.1093/mnras/stac2947, arXiv:2204.06302 [astro-ph.CO].
- [25] J. M. Wagstaff and R. Banerjee, *Phys. Rev. D* **92**, 123004 (2015), arXiv:1508.01683 [astro-ph.CO].
- [26] K. Jedamzik, V. Katalinic, and A. V. Olinto, *Phys. Rev. Lett.* **85**, 700 (2000), arXiv:astro-ph/9911100.
- [27] P. A. R. Ade *et al.* (Planck), *Astron. Astrophys.* **594**, A19 (2016), arXiv:1502.01594 [astro-ph.CO].
- [28] D. Paoletti and F. Finelli, *JCAP* **11**, 028 (2019), arXiv:1910.07456 [astro-ph.CO].
- [29] D. Paoletti *et al.* (LiteBIRD), *JCAP* **07**, 086 (2024), arXiv:2403.16763 [astro-ph.CO].
- [30] I. Wasserman, *ApJ* **224**, 337 (1978).
- [31] E.-j. Kim, A. Olinto, and R. Rosner, *Astrophys. J.* **468**, 28 (1996), arXiv:astro-ph/9412070.
- [32] K. Subramanian and J. D. Barrow, *Phys. Rev. D* **58**, 083502 (1998), arXiv:astro-ph/9712083.
- [33] J. R. Shaw and A. Lewis, *Phys. Rev. D* **86**, 043510 (2012), arXiv:1006.4242 [astro-ph.CO].
- [34] C. Fedeli and L. Moscardini, *JCAP* **2012**, 055 (2012), arXiv:1209.6332 [astro-ph.CO].
- [35] K. L. Pandey and S. K. Sethi, *ApJ* **762**, 15 (2013), arXiv:1210.3298 [astro-ph.CO].
- [36] S. Chongchitnan and A. Meiksin, *Mon. Not. Roy. Astron. Soc.* **437**, 3639 (2014), arXiv:1311.1504 [astro-ph.CO].
- [37] T. Kahniashvili, Y. Maravin, A. Natarajan, N. Battaglia, and A. G. Tevzadze, *ApJ* **770**, 47 (2013), arXiv:1211.2769 [astro-ph.CO].
- [38] D. Montanino, F. Vazza, A. Mirizzi, and M. Viel, *Phys. Rev. Lett.* **119**, 101101 (2017), arXiv:1703.07314 [astro-ph.HE].
- [39] M. Sanati, Y. Revaz, J. Schober, K. E. Kunze, and P. Jablonka, *Astronomy and Astrophysics* **643**, A54 (2020).
- [40] M. Sanati, S. Martin-Alvarez, J. Schober, Y. Revaz, A. Slyz, and J. Devriendt, (2024), arXiv:2403.05672 [astro-ph.GA].
- [41] Q. Zhang, S. Li, X.-H. Tan, and J.-Q. Xia, (2024), arXiv:2408.03584 [astro-ph.CO].
- [42] H. Katz, S. Martin-Alvarez, J. Rosdahl, T. Kimm, J. Blaizot, M. G. Haehnelt, L. Michel-Dansac, T. Garel, J. Oñorbe, J. Devriendt, A. Slyz, O. Attia, and R. Teyssier, *Mon. Not. Roy. Astron. Soc.* **507**, 1254 (2021), arXiv:2101.11624 [astro-ph.CO].

- [43] H. Tashiro and N. Sugiyama, *Mon. Not. Roy. Astron. Soc.* **368**, 965 (2006), arXiv:astro-ph/0512626 [astro-ph].
- [44] S. K. Sethi and K. Subramanian, *Mon. Not. Roy. Astron. Soc.* **356**, 778 (2005), arXiv:astro-ph/0405413.
- [45] K. L. Pandey, T. R. Choudhury, S. K. Sethi, and A. Ferrara, *Mon. Not. Roy. Astron. Soc.* **451**, 1692 (2015), arXiv:1410.0368 [astro-ph.CO].
- [46] H. A. G. Cruz, T. Adi, J. Flitter, M. Kamionkowski, and E. D. Kovetz, (2023), arXiv:2308.04483 [astro-ph.CO].
- [47] A. Bhaumik, D. Paul, and S. Pal, (2024), arXiv:2407.11923 [astro-ph.CO].
- [48] T. Adi, H. A. G. Cruz, and M. Kamionkowski, *Phys. Rev. D* **108**, 023521 (2023), arXiv:2306.11319 [astro-ph.CO].
- [49] D. R. G. Schleicher, R. Banerjee, and R. S. Klessen, *Astrophys. J.* **692**, 236 (2009), arXiv:0808.1461 [astro-ph].
- [50] P. Ralegankar, M. Pavičević, and M. Viel, *JCAP* **07**, 027 (2024), arXiv:2402.14079 [astro-ph.CO].
- [51] P. Ralegankar, E. Garaldi, and M. Viel, (2024), arXiv:2410.02676 [astro-ph.CO].
- [52] M. Pavičević, V. Iršič, M. Viel, J. Bolton, M. G. Haehnelt, S. Martin-Alvarez, E. Puchwein, and P. Ralegankar, (2025), arXiv:2501.06299 [astro-ph.CO].
- [53] A. Roper Pol, C. Caprini, A. Neronov, and D. Semikoz, *Phys. Rev. D* **105**, 123502 (2022), arXiv:2201.05630 [astro-ph.CO].
- [54] A. Roper Pol, in *56th Rencontres de Moriond on Gravitation* (2022) arXiv:2205.09261 [gr-qc].
- [55] S. Balaji, M. Fairbairn, and M. O. Olea-Romacho, *Phys. Rev. D* **109**, 075048 (2024), arXiv:2402.05179 [hep-ph].
- [56] A. G. Riess, S. Casertano, W. Yuan, J. B. Bowers, L. Macri, J. C. Zinn, and D. Scolnic, *Astrophys. J. Lett.* **908**, L6 (2021), arXiv:2012.08534 [astro-ph.CO].
- [57] N. Aghanim *et al.* (Planck), *Astron. Astrophys.* **641**, A6 (2020), [Erratum: *Astron. Astrophys.* 652, C4 (2021)], arXiv:1807.06209 [astro-ph.CO].
- [58] K. Jedamzik, L. Pogosian, and T. Abel, (2025), arXiv:2503.09599 [astro-ph.CO].
- [59] K. Jedamzik and L. Pogosian, *Phys. Rev. Lett.* **125**, 181302 (2020), arXiv:2004.09487 [astro-ph.CO].
- [60] P. Ralegankar, *Phys. Rev. Lett.* **131**, 231002 (2023), arXiv:2303.11861 [astro-ph.CO].
- [61] J. Aalbers *et al.* (LZ), (2024), arXiv:2410.17036 [hep-ex].
- [62] M. Crnogorčević, M. S. Delos, N. Kuritzén, and T. Linden, (2025), arXiv:2501.14865 [astro-ph.HE].
- [63] M. S. Delos and S. D. M. White, *JCAP* **10**, 008 (2023), arXiv:2209.11237 [astro-ph.CO].
- [64] A. Brandenburg, R. Sharma, and T. Vachaspati, *J. Plasma Phys.* **89**, 905890606 (2023), arXiv:2307.04602 [physics.plasm-ph].
- [65] A. M. Green, S. Hofmann, and D. J. Schwarz, *JCAP* **08**, 003 (2005), arXiv:astro-ph/0503387.
- [66] C. Gross, O. Lebedev, and T. Toma, *Phys. Rev. Lett.* **119**, 191801 (2017), arXiv:1708.02253 [hep-ph].
- [67] G. Arcadi and S. Profumo, (2025), arXiv:2506.19062 [hep-ph].
- [68] T. Abe, *Phys. Rev. D* **104**, 035025 (2021), arXiv:2106.01956 [hep-ph].
- [69] M. S. Delos, M. Bruff, and A. L. Erickcek, *Phys. Rev. D* **100**, 023523 (2019), arXiv:1905.05766 [astro-ph.CO].
- [70] M. S. Delos and S. D. M. White, *Mon. Not. Roy. Astron. Soc.* **518**, 3509 (2022), arXiv:2207.05082 [astro-ph.CO].
- [71] A. V. Maccio, S. Paduroiu, D. Anderhalden, A. Schneider, and B. Moore, *Mon. Not. Roy. Astron. Soc.* **424**, 1105 (2012), arXiv:1202.1282 [astro-ph.CO].
- [72] R. K. Sheth, H. J. Mo, and G. Tormen, *Mon. Not. Roy. Astron. Soc.* **323**, 1 (2001), arXiv:astro-ph/9907024.
- [73] J. M. Bardeen, J. R. Bond, N. Kaiser, and A. S. Szalay, *Astrophys. J.* **304**, 15 (1986).
- [74] M. Di Mauro, J. Pérez-Romero, M. A. Sánchez-Conde, and N. Fornengo, *Phys. Rev. D* **107**, 083030 (2023), arXiv:2303.16930 [astro-ph.HE].
- [75] D. N. Hosking and A. A. Schekochihin, (2022), arXiv:2203.03573 [astro-ph.CO].
- [76] R. Banerjee and K. Jedamzik, *Phys. Rev. D* **70**, 123003 (2004), arXiv:astro-ph/0410032.
- [77] A. Acharyya *et al.* (CTA), *JCAP* **01**, 057 (2021), arXiv:2007.16129 [astro-ph.HE].